Mechanical Systems and Signal Processing 154 (2021) 107550

Contents lists available at ScienceDirect

Mechanical Systems and Signal Processing

journal homepage: www.elsevier.com/locate/ymssp

In situ wireless measurement of grinding force in silicon wafer self-rotating grinding process

Fei Qin [a,b], Lixiang Zhang [a], Pei Chen [a,b,*], Tong An [a], Yanwei Dai [a], Yanpeng Gong [a], Zhongbo Yi [c], Haiming Wang [c]

[a] Institute of Electronics Packaging Technology & Reliability, Faculty of Materials and Manufacturing, Beijing University of Technology, Beijing 100124, China
[b] Beijing Key Laboratory of Advanced Manufacturing Technology, Faculty of Materials and Manufacturing, Beijing University of Technology, Beijing 100124, China
[c] The 45th Research Institute of China Electronic Technology Corporation, Beijing 100176, China

ARTICLE INFO

Article history:
Received 16 July 2020
Received in revised form 10 November 2020
Accepted 18 December 2020

Keywords:
Silicon wafer
Self-rotating grinding
Grinding force
Materials removal
Specific grinding energy
Process parameter

ABSTRACT

Grinding force is a crucial factor that affects the machining accuracy, wheel wear and the material removal efficiency for precision machining of semiconductor materials under nanometer accuracy. However, due to the complex rotational motion of both the grinding wheel and wafer workpiece, in situ measurement of the grinding force in wafer self-rotating grinding is still a big challenge. In this paper, a novel grinding force measurement method in silicon wafer grinding process is developed. The method is achieved by embedding four thin film force sensors into a self-designed force measurement device and real-time monitoring through wireless signal transmission. Based on this method, the grinding force under 5 groups of process parameters are measured. For the first time, the variations of grinding force during the whole grinding process are revealed real-timely. Effects of process parameters, i.e. spindle rotational speed and feed rate, on grinding force are investigated, and the parameters are also optimized based on the theory of specific grinding energy. The test results show that the force measurement method has the advantages of high precision, reliable and convenient implementation.

1. Introduction

Monocrystalline silicon wafer is the dominant substrate material for integrated circuit (IC) manufacturing [1]. During industrial processing of silicon, grinding is commonly used as the last "rough" machining process prior to high-precision polishing/etching process, because grinding can achieve high material removal rate with relatively low cost. However, these advantages are accompanied by machining damage on wafer, e.g. surface/subsurface micro-crack [2,3], due to the brittle nature of silicon. Higher quality and productivity require the optimum selection of process parameters to utilize the full potential of the grinding process. In the last decades, lots of attempts have been made to reduce the surface/subsurface damage by optimizing the process parameters. For example, Sun and Zhang [4,5] established the relationship between the surface roughness/subsurface damage depth and process parameters, and tried to reduce the damage through the optimization of processing parameters. However, until now, the damage factors are not directly connected with processing parameters

* Corresponding author at: Institute of Electronics Packaging Technology & Reliability, Faculty of Materials and Manufacturing, Beijing University of Technology, Beijing 100124, China.
E-mail address: peichen@bjut.edu.cn (P. Chen).

https://doi.org/10.1016/j.ymssp.2020.107550
0888-3270/

experimentally, and most of the research work is still empirical studies. Since the grinding force is an essential factor to connect input of parameter and output of wafer quality, which has not been measured properly yet.

Furthermore, with the development of electronic packaging technology in recent years, grinding attracts more interests in various applications, e.g. three-dimensional (3D) integration packaging and micro-electro-mechanical system (MEMS) [6,7]. The silicon wafer needs to be thinned from the back side after the fabrication of the copper pillar bump or Ball Grid Array (BGA) [8]. Due to the existence of the heterostructure, the ultra-thin wafer might crack under the action of the grinding force. Therefore, in situ measurement of the grinding force is truly meaningful to understand the complex brittle material removal process, which enables throughput improvement, inline quality analysis and manufacturing costs reduction.

Actually, a lot of work has been done for the measurement of the grinding force in the traditional grinding process and various kinds of grinding force sensors have been developed [9]. Among which, the most widely used sensor is the piezoelectric sensor [10,11]. Durgumahanti et al. [12] measured the grinding force in surface grinding process by using the piezoelectric sensor, and revealed that the grinding force increased with the cutting depth and decreased with the wheel speed. Li et al. [13] monitored the grinding force in micro grinding of RB-SiC (Reaction Bonded Silicon Carbide) ceramic and indicated that the grinding force increased with the feed rate of workpiece. These sensors are mature and of high measurement accuracy and repeatability, but those sensors have large size, which cannot be embedded in the rotating chuck table. At present, the industry mainly monitors the grinding process by measuring the current or power of the motor [14,15]. This is an indirect measurement method to reflect the relative magnitude of grinding force without any reformation, furthermore, the accurate of this method is far less than direct methods [16].

With the development of micro-fabrication technology, the schemes that integrating small sensors into grinding wheel or workpiece have been proposed [17,18]. These sensors include semi-conductive strain gauge, piezoelectric sensors, thin film force sensors, etc. Sarma [19] developed a sensor-integrated workpiece for in situ measurement of strain during cylindrical grinding process. By integrating a piezoelectric sensing element in size of 8×8 mm^2 into the grinding wheel, Brinksmeier [18] measured the grinding force in external cylindrical grinding process. Zhao [20] developed a semi-conductive strain gauge based on the MEMS manufacturing technology, and used it for force measurement in cutting process. Due to the small size, these sensors can be compactly integrated with existing equipment and fixtures for force measurement through wire or wireless approach. However, these sensors need special manufacturing, the manufacturing process is complex, and the reliability may not be high. Ma at al. [21,22] mounted the PVDF strain sensor to the end of the milling cutter and measured the cutting forces in peripheral end milling process. The thickness of the thin film sensor can be reduced to several hundred microns, which is considered to be the promising candidate for force measurement. Luo et al. [23] monitored the cutting force applied on each cutting edge by embedding the piezoelectric thin film force senor in each insert. Liu et al. [24] measured the milling force of aircraft structure by embedding thin-film sensors integrated into a fixture system.

However, all of the above force measurement studies are based on the conventional machining process. For silicon wafer self-rotating grinding process, the chuck table and the grinding wheel rotate about their own axes, the wafer is ground as the rotating grinding wheel moving downward. By integrating the capacitive displacement sensor into the workpiece spindle, Couey [25] monitored the normal grinding force of the spindle. However, during the material removal, the amount of material removed along the wafer radius changes, the grinding force should also be different. The normal spindle force is the sum of grinding force in the contact zone, which cannot reflect the distribution of the grinding force on different location of the wafer. By integrating the piezoelectric sensor under the wheel segment, Pahler [26] captured the grinding force on the wheel segment, and reveals the variation of the grinding force along wafer radial distance. However, this approach of force measurement introduced additional structural compliance in the structure loop, and produced inhomogeneous centrifugal force, which are different from the actual grinding process. In addition, since the spindle speed is far greater than the wafer speed, sampling frequency of wireless transmission needs to be much higher if installing the sensor on the spindle. Therefore, sensor under wafer is a solution to the structural compliance change, inhomogeneous centrifugal force and enough sampling frequency.

In this paper, a novel in situ grinding force measurement device and method in silicon wafer self-rotating grinding process is developed. The basic idea is to replace the back grinding (BG) tape with thin film force sensor to obtain the force signal and transmit it to a computer terminal wirelessly. Four thin film force sensors, based on the piezo-resistive properties of graphite materials, are embedded beneath the silicon wafer along the radial distance through a special designed force measurement device. Based on the proposed method, variations of grinding force during the whole grinding process are revealed. Effects of process parameters on grinding force are also investigated. A process parameter optimization method aiming to reduce grinding damage and improve machining efficiency is also proposed base on the experimental results.

2. Experimental

2.1. Testing device and method

The self-designed grinding force measurement system is illustrated in Fig. 1 (a), which mainly consists of two parts, the grinding force measurement device and wireless transmission system. The diameter and thickness of the grinding force test device are 230 mm and 55 mm, which is mounted on the vacuum chuck table. During the grinding process, the vacuum chuck and grinding wheel rotate about their own axle along same direction. The vacuum chuck is slightly convex and has

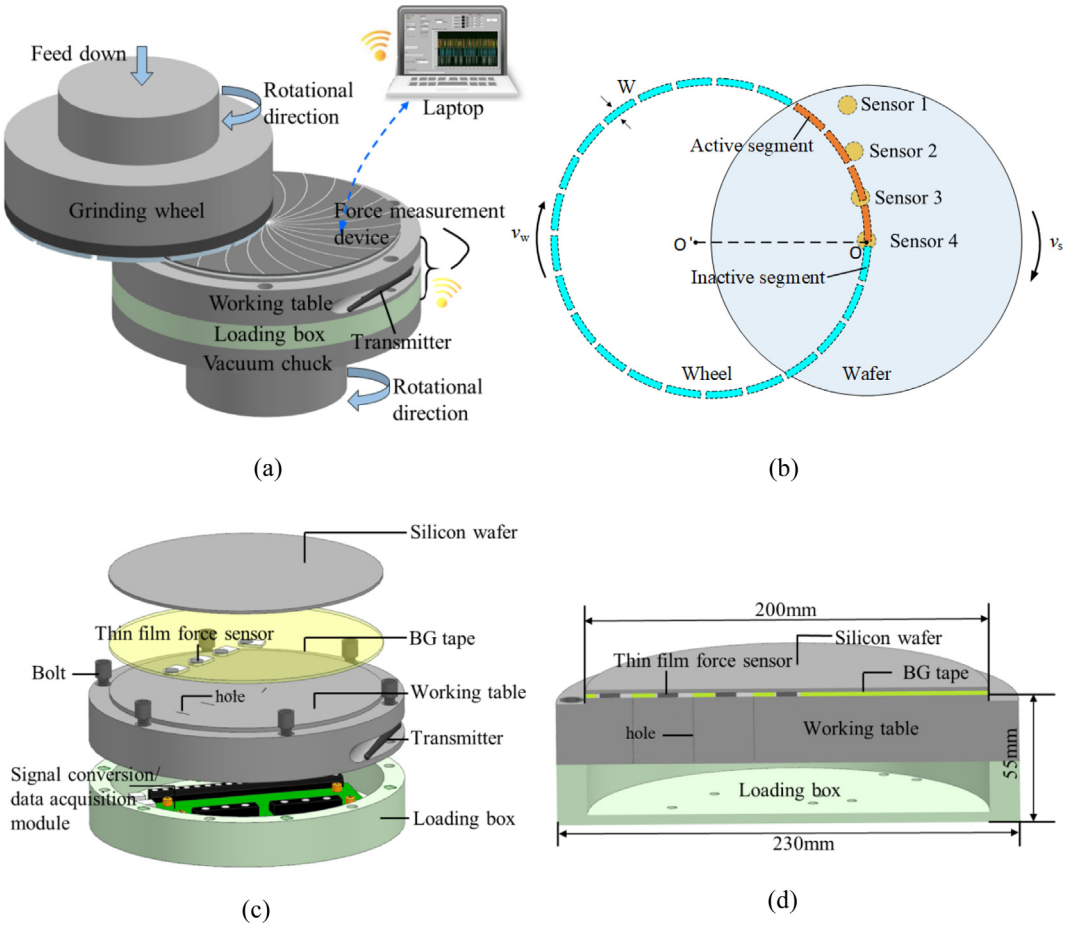

Fig. 1. Schematic diagram of the grinding force measurement system. (a) Grinding force measurement system; (b) Top view of the rotating wafer and grinding wheel; (c) Force measurement unit; (d) Cross-section of the force measurement unit.

a certain inclination angle with the grinding wheel axis. When the grinding wheel feed downward, less than a quarter of the grinding wheel contacts with the wafer, as shown by wheel segments with yellow color in Fig. 1 (b).

The grinding force measurement unit is shown in Fig. 1 (c) & (d), which consists of thin film force sensor, working table, loading box and data acquisition/processing module. Considering that the distance between sensors should be greater than half of wheel segment (15 mm) plus the radius of the sensor (5 mm), i.e. 20 mm, four of thin film force sensors are embedded beneath the wafer with radial distance of 0, 30, 60, 90 mm. The silicon wafer is bonded with the working table through BG tape with the thickness of 0.21 mm, which has the same thickness as the thin film force sensor. The connecting wires of the sensors passes the through hole of the working table and is connected with the data acquisition and processing module in the loading box. When the grinding wheel feeds downwards, the contact force between the grinding wheel and the wafer will also be transferred to the sensor, and the electronical resistance of the sensor will change. And then, the resistance-to-voltage conversion module is used to convert the force signal into the output voltage. After the analogue-to-digital conversion, the output signals of the sensors are transmitted by the wireless transmitter, which located on the side of the working table.

Fig. 2 shows the mounting of grinding force measuring system on an automatic wafer grinding and polishing machine (WGP-300, CETC, China) (Fig. 2 (a)), which consists of three spindles including rough grinding, fine grinding and dry polishing spindles. In current study, the rough grinding spindle (grinding wheel with mesh size of 320) was selected, as shown in Fig. 2 (b). The real setup of the grinding force measurement unit is shown in Fig. 2(c). The commercially available thin film force sensors (Flexiforce A201, Tekscan, USA) used in this paper is based on the piezo-resistive characteristics of graphite ink. The diameter of the force sensitive area is 9.5 mm and the thickness is 0.21 mm [27].

The resistance-to-voltage conversion module was used to convert the variation of the resistance signal into the output voltage with LM393 comparator, as shown in Fig. 2(c). After that, output voltage signals are collected by 16-bit high speed analog to digital converter (16-bit high speed ADC) by a data acquisition card (Labjack T7 pro, USA), which has an analog input resolution of 1 μV noise-free and maximum 14-channel analog inputs. Processed signals are then sent to a high-

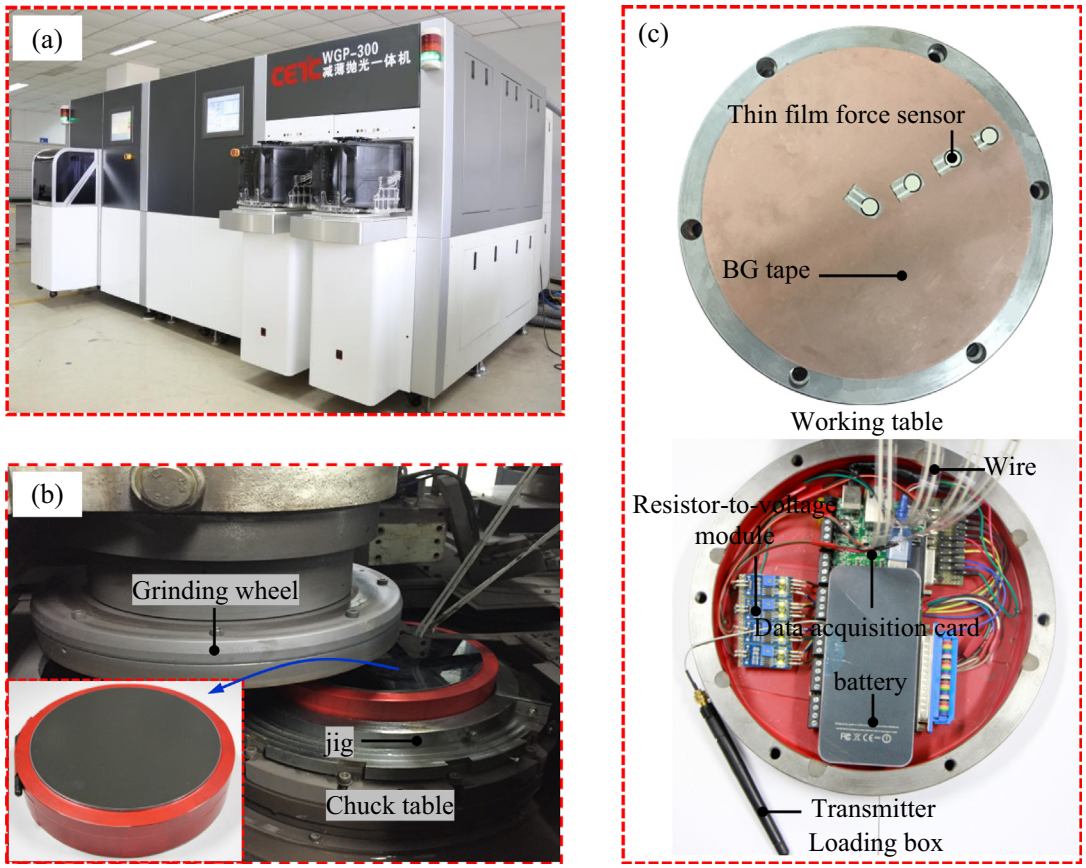

Fig. 2. Setup of the grinding force measuring system, (a) grinding machine; (b) configuration of grinding force measuring device; (c) integrated force measurement device with thin film sensor.

speed DSP processer, which will then send the digital signals to the transmitter. The wireless transfer is realized by Wireless Fidelity (WIFI) protocol with a sampling frequency of 2000 Hz. The power supply of the test system is realized by a 5 V lithium battery.

2.2. Calibration

The purpose of this study is to measure the grinding force of a single segment of grinding wheel that applied on the ground wafer surface, however, in our scheme, the sensors are embedded beneath the silicon wafer. Therefore, calibration is needed to establish the relationship between the force applied by a single wheel segment and the output signal of the sensor. Considering that the wheel segments and sensors are in motion during grinding, the calibration test should also be locational dependent. For this, a schematic time-travel-output voltage relationship was established first, and then a special designed calibration experiment was performed to obtain the relationship between the output voltage of the sensor and the loading force on the wheel segment.

Fig. 3 (a) illustrates the schematic diagram of the movement process of the grinding wheel and wafer. Every time, when the chuck table rotation for a cycle, the force sensors pass beneath the wheel segment and one cycle of the measurement is achieved. For the sensors located on the outer circumference of the wafer (sensor 1 to sensor 3), the relative motion of the wheel segment and the output voltage can be shown in Fig. 3 (b). When the wheel segments are close to the sensors (t_0 to t_2), the output voltage increases; when the wheel segments are away from the sensors, the output voltage decreases (t_2 to t_4). When the gravity center of the wheel segment is superposed on the center position of the sensor, the output signal is the largest. For the sensors located on the center of the wafer (sensor 4), the relative motion of the wheel segment and the output voltage are shown in Fig. 3 (c). The wheel segment is always in contact with half of the sensor. Because the wheel segment is always central symmetry at different moment, the output voltage of the sensor should be the same.

The calibration test was performed on the assembled force measurement device, and a dynamic normal force is used with a mechanical micro tester (Instron 5948, USA). In order to be consistent with the grinding conditions, the indenter with the same shape as the wheel segment (segment with length of 30 mm and width of 3.5 mm) is adopted, as shown in Fig. 4. For

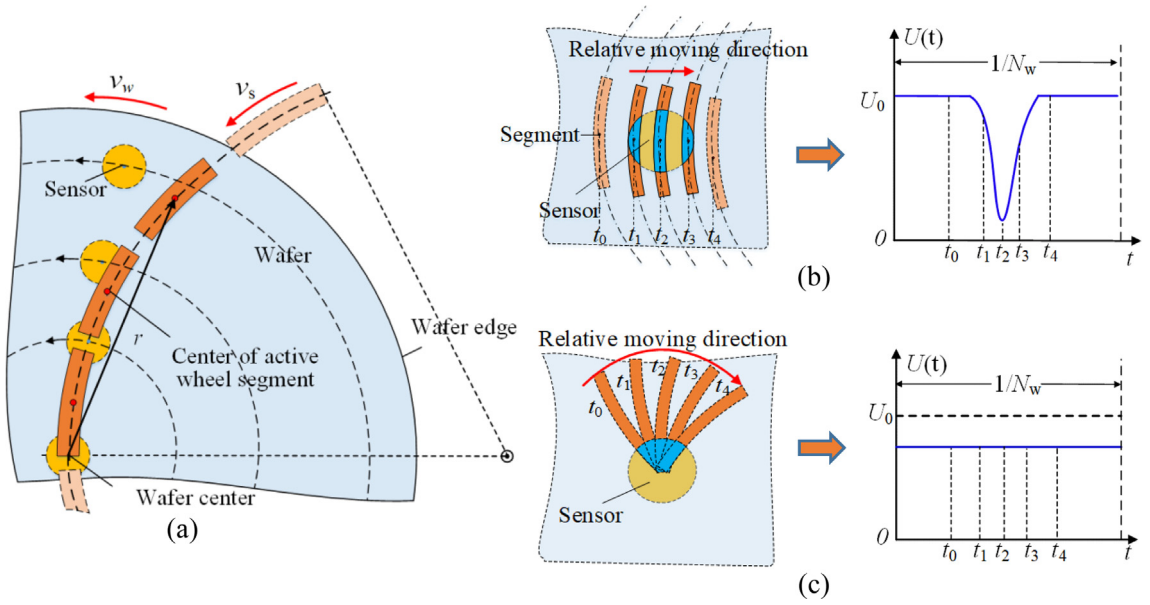

Fig. 3. Schematic diagram of time-travel-output voltage during grinding process, (a) moving process of the grinding wheel segments, (b) sensor output signal. Relationship between segment sensor 1 to sensor 3 and (c) sensor 4.

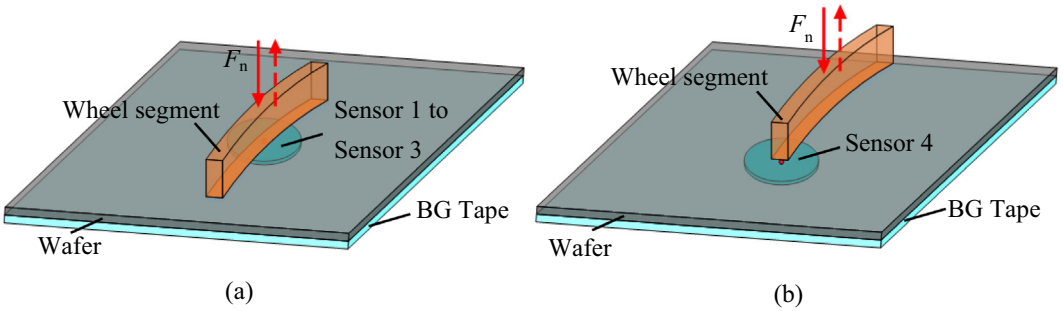

Fig. 4. Schematic diagram of the dynamic calibration. (a) Calibration scheme of sensor 1 to sensor 3; (b) calibration scheme of sensor 4.

the sensors located on the outer circumference of the wafer (sensor 1 to sensor 3), the gravity center of the wheel segment is consistent with the center position of the sensor, as shown in Fig. 4 (a). For the sensor located in the center of the wafer (sensor 4), the wheel segment is in contact with half of the sensor, as shown in Fig. 4 (b). Considering the output voltage difference between the four sensors, and the pre-pressure may vary slightly for different sensors in the process of wafer bonding, the sensors are calibrated separately. The maximum normal force of 100 N is used. For one sensor, each calibration is carried out with three loading cycles.

Fig. 5 shows the calibration results of the four thin film force sensors. The dynamic response of the measurement system with the loading force is shown in the inner figure of Fig. 5. Taking sensor 1 (Fig. 5 (a)) as an example, the loading force is shown in black color and the response of the thin film force sensor is shown in blue color. The output voltage of sensors decreases as the applied force increases, and shows good consistency with the loading force. The relationship between voltage output and the applied force can be derived by fitting the data as,

$$\boldsymbol{Y} = \boldsymbol{A} \cdot \boldsymbol{X} + \boldsymbol{B}$$

where $\boldsymbol{A}$ = $[-71.93, -71.68, -71.42, -107.52]^T$, and $\boldsymbol{B}$ = $[352.95, 352.22, 353.92, 541.18]^T$. $\boldsymbol{X}$ is the output voltage of the sensor and $\boldsymbol{Y}$ is the loading force obtained from the micro tester. The linearity, hysteresis, and repeatability of the four sensors in the embedded system are calculated and listed in Table 1, which represent the accuracy and precision of the measurement.

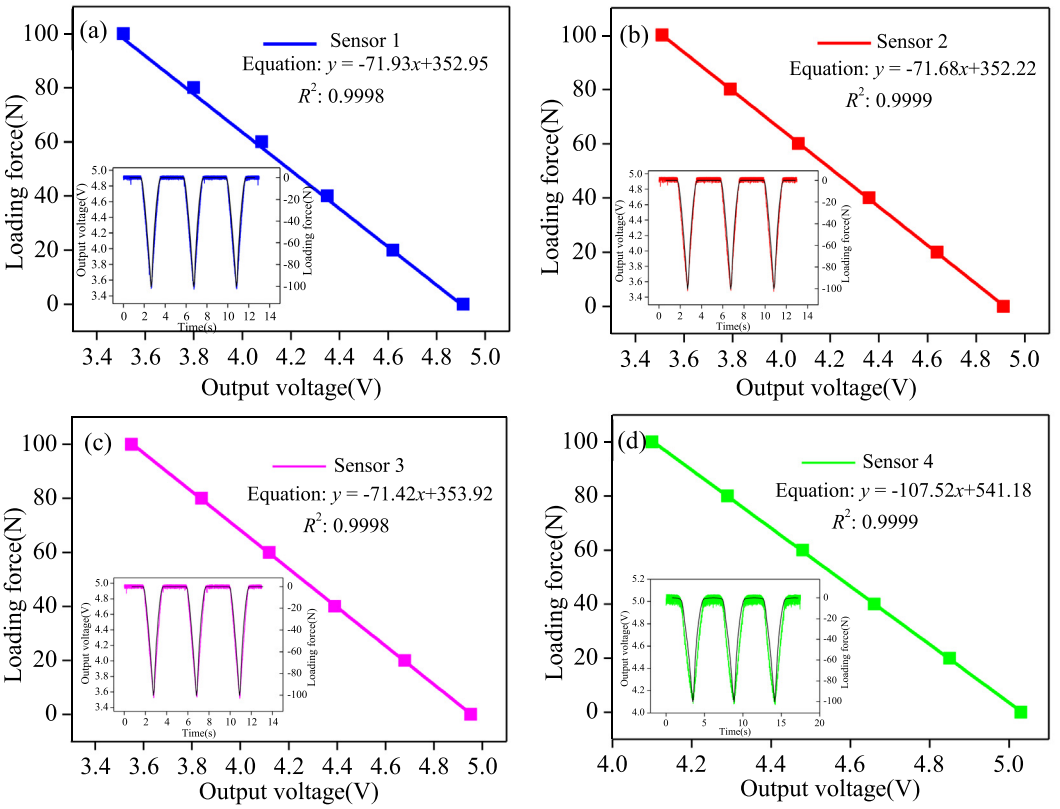

Fig. 5. Calibration results of the force sensors. (a) Sensor 1; (b) sensor 2; (c) sensor 3; (d) sensor 4.

Table 1
Accuracy and precision of the four sensors in the embedded system.

Performance	Sensor 1	Sensor 2	Sensor 3	Sensor4
Linearity	4.00%	5.23%	4.84%	7.41%
Hysteresis	2.78%	3.17%	2.73%	6.63%
Repeatability	1.29%	2.04%	1.35%	3.59%

2.3. Grinding procedure with varied process parameters

The calibrated test fixture was mounted on the grinding machine, and 8-inch silicon wafer was bonded on the fixture for real grinding process. The wafer is set to remove 250 μm in thickness during whole grinding process. The process parameters used for the grinding experiment are listed in Table 2, which considered the effects of spindle feed rate and spindle rotational speed on the grinding force. Resin bond cup-type grinding wheel with outer diameter of 313 m is adopted for the text. The length and width of a wheel segment are 30 mm and 3.5 mm, the gap length between the wheel segment is 5 mm. During grinding process, deionized water is used to diffuse the heat generated by grinding. The deionized water comes in two ways, one is from the outlets in grinding wheel. The other is from the water pipes. By both ways, the water flows on the wafer surface without any pressure.

Table 2
Process parameters.

Condition	Feed rate f(μm/min)	Spindle rotational speed N_w(r/min)	Wafer rotational speed N_s(r/min)
(a)	90	3000	100
(b)	60	3000	100
(c)	30	3000	100
(d)	60	2500	100
(e)	60	2000	100

3. Results and discussion

3.1. Rationality and repeatability of the force measurement

Fig. 6 (a) illustrates the schematic diagram of the movement process of the grinding wheel and wafer. Periodically, when the wafer rotates for one cycle, the force sensors pass beneath the wheel segment and one cycle of measurement is achieved. As shown in Fig. 6 (a), in one rotation, sensor 1 comes into contacting with the grinding wheel first, then sensors 2 and 3. Sensor 4 is always in contact with the grinding wheel during the whole process. Fig. 6 (b) shows grinding force of the four sensors to time in one cycle of wafer rotation under condition (b). Clearly, when the force sensor far from the wheel segment, the grinding force measured by the sensor 1 to sensor 3 is zero. With the wafer rotating, the grinding force of sensor 1 has a sharp drop and reaches the peak value first, then followed by sensor 2 and then sensor 3. The output voltage of sensor 4 is always offset from the initial value as it is always under contact with the wheel segments.

The moments when the gravity center of wheel segment moves to superpose the center of sensor 1, sensor 2 and sensor 3 are defined as t_{s1}, t_{s2} and t_{s3}, respectively. For the process parameter set in the test, the interval time ($\Delta t_1 = t_{s2} - t_{s1}$) between the wheel segment moves from the sensor 1 to the sensor 2 can be calculated by the geometric dimension and the rotating speed of wafer, which is about 10 ms, and the interval time ($\Delta t_2 = t_{s3} - t_{s1}$) between sensor 1 and sensor 3 is about 20 ms. As shown in Fig. 6 (b), the measured interval time of Δt_1 and Δt_2 are also about 10 ms and 20 ms. It is consistent to the actual grinding process.

Fig. 7 (a) to (d) further show the measurement data of the four sensors during the grinding process. In each figure, 6 cycles of measurement data are displayed. The interval time between two adjacent pulses is 0.6 s, that is the time the wafer rotates for one cycle. For the sensor 1 to 3, the grinding force signal shows good repeatability. For sensor 4, the grinding force signal also shows good repeatability for different cycle. However, for a signal cycle, the grinding force fluctuates, and shows larger variation. The vibration of the wheel and the discreteness of abrasive grain in the wheel, may cause the force variation on the sensor 4. Furthermore, the grind wheel cannot be exactly allied in the center, therefore, at different time, there will be a periodical variation during one rotation of grinding wheel, which is another source of the amplitude variation. However, the same periodical variation as other three sensors is also indicated that the method of grinding force measurement is reliable.

3.2. Variation of the grinding force over grinding process

Fig. 8 illustrates the force variation of one of the four sensors under condition (b) (sensor 1, r = 90 mm). Fig. 8 (a)–(c) are the original record of grinding force at different grinding stages, Fig. 8(d) shows the force and wheel feed depth over the whole grinding process. Each data point in Fig. 8 (d) represents the value of each pulse signal and the results of Fig. 8 (a)–(c) correspond to the "A", "B" and "C" marked in Fig. 8 (d).

As shown in Fig. 8, the whole grinding process can be divided into three stages: the initial contact stage, the stable removal stage, and the end stage. The grinding force is zero prior to the grinding wheel contacting with the silicon wafer. With the downward feed of the grinding wheel, the grinding wheel engages with the wafer, which is named the initial contact stage, and the grinding force begins to increase. After about 60 s, the grinding force climbs to about 77.65 N for this set of process parameters. The grinding force and the feed of grinding wheel reach a stable plateau. When the feed depth of grind-

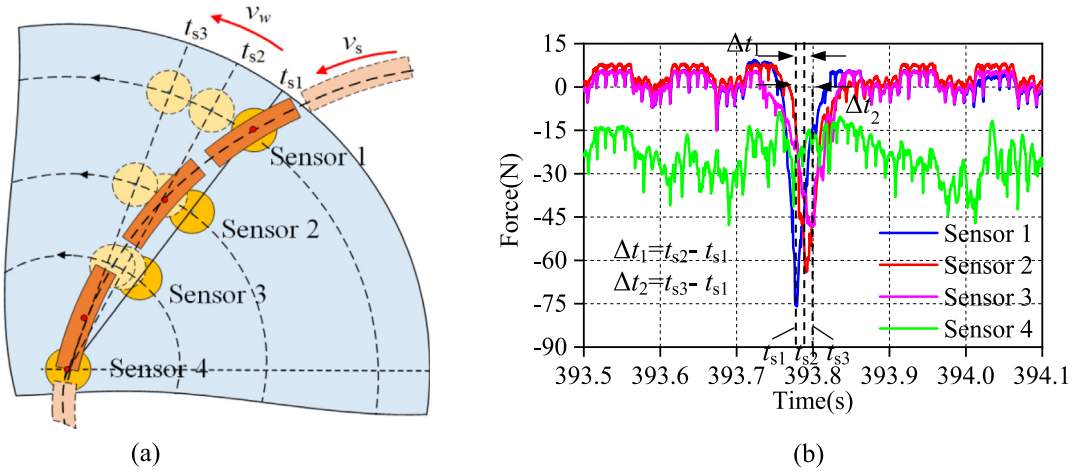

Fig. 6. Time-travel grinding force relationship during one cycle of wafer rotation. (a) Time-travel relationship between the sensor and grinding wheel; (b) Force variation by the four sensors during one cycle of wafer rotation under condition (b).

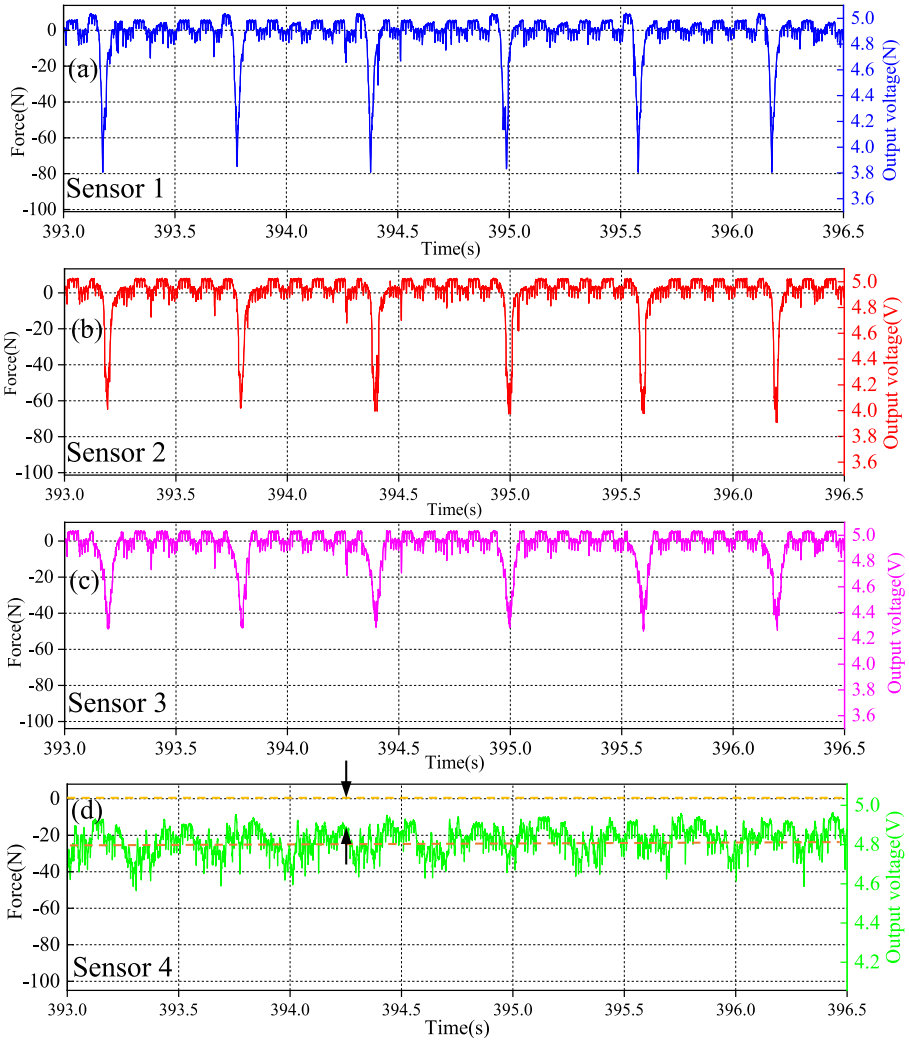

Fig. 7. Original record force signal of the four sensors under condition (b). (a) Sensor 1; (b) sensor 2; (c) sensor 3; (d) sensor 4.

ing wheel reaches the target of 250 μm, the grinding wheel retracts quickly, and the grinding force changes to zero, the whole grinding process is done.

The force variation of sensor 4 during grinding process is shown in Fig. 9. Fig. 9 (a) and (b) are the original record of grinding force in the initial contact stage, the stable remove stage and the end stage corresponding to the range A and B in Fig. 9 (c). As expected, since the grinding wheel and sensor are always in contact, the change of force is continuous, as shown in Fig. 9 (a) and (b). In the initial contact stage of the grinding process, as shown in Fig. 9 (a), the grinding force changes periodically and increases slowly with the feed of grinding wheel. With the increase of the feed depth of the grinding wheel, the grinding force tends to be stable and the periodic trend gradually disappears, as shown in Fig. 9 (b). In the end stage of grinding, the grinding force decreases continuously, and the grinding wheel leaves the wafer within 0.55 s.

3.3. Effects of process parameters on grinding force

The measurement results of grinding force in stable removal stage under different process parameters are listed in Table 3. For the process parameters selected in this paper, the measured force is in the range of 17.51 N to 90.60 N. For all of the five process conditions, by increasing the radial distance of the wafer, the grinding force are increased constantly.

Fig. 10 illustrate the effects of process parameters, i.e. spindle rotational speed (Fig. 10 (a)), wheel feed rate (Fig. 10 (b)), on grinding force. As shown in Fig. 10 (a), when the feed rate and the wafer rotating speed remain constant, the grinding force decreases from 86.47 N to 77.65 N (sensor 1), 73.06–67.90 N (sensor 2), as the spindle speed increases from 2000 rpm to 3000 rpm. It shows that the grinding force decreases with the spindle rotational speed increase. When the rotational speeds of the spindle and wafer are remains constant (shown in Fig. 10(b)), the grinding force increases from 70.03 N

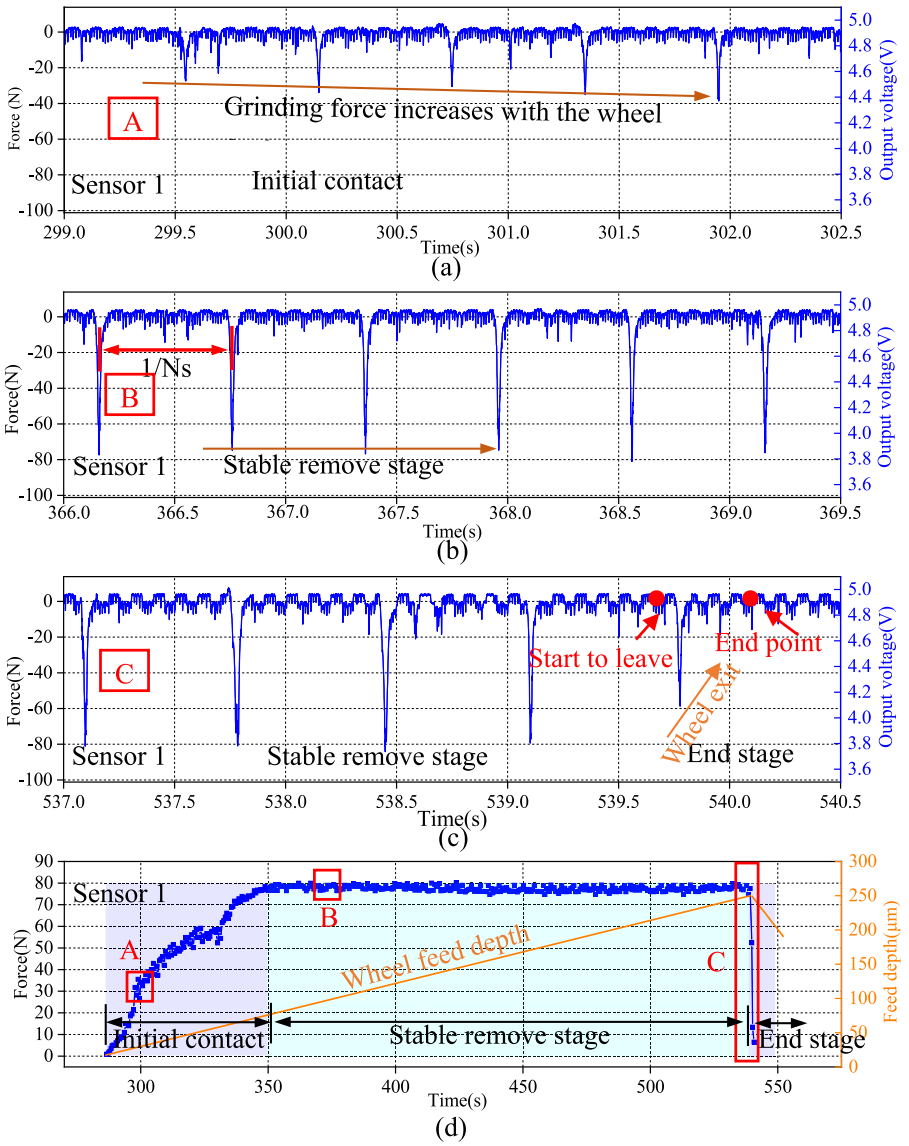

Fig. 8. Force variation of sensor 1 under condition (b). (a) initial stage; (b) stable removal stage; (c) end stage; (d) variation of the grinding force in the whole grinding stages.

to 90.60 N (sensor 1), 50.32–73.40 N (sensor 2), as the wheel feed rate increases from 30 μm/min to 90 μm/min. It shows that grinding force increases with the wheel feed rate.

Actually, the effects of process parameters on grinding force are related to the local removal of materials. Fig. 11 shows a schematic diagram of local material removal in wafer self-rotating grinding process. When the grinding wheel rotates for one cycle, the area swept by the grinding wheel is a sector shown in Fig. 11 (a). For a single wheel segment at radial distance r, the local removal amount can be simplified as a trapezoid with inner radius r_i and outer radius r_o, as shown in Fig. 11 (b). It can be expressed as,

$$V = \int_{r_i}^{r_o} B\mathrm{d}r = \int_{r_i}^{r_o} \frac{2\pi r \cdot N_w}{N_s} \cdot \frac{f}{N_w}\mathrm{d}r = \frac{\pi(r_o^2 - r_i^2)\cdot f}{N_s} = \frac{2\pi r_s \cdot f}{N_s}(l_s + l_g) \tag{1}$$

where r is the radial distance of the wafer, r_s is the distance from the center of active wheel segment to wafer center. N_w and N_s are the rotational speeds of the spindle and wafer respectively, f is the wheel feed rate. $2\pi r_s N_w/N_s$ is the wheel span width at wafer radial r, f/N_w is the material removal thickness. l_s is the length of the wheel segment, l_g is the gap length between the segments.

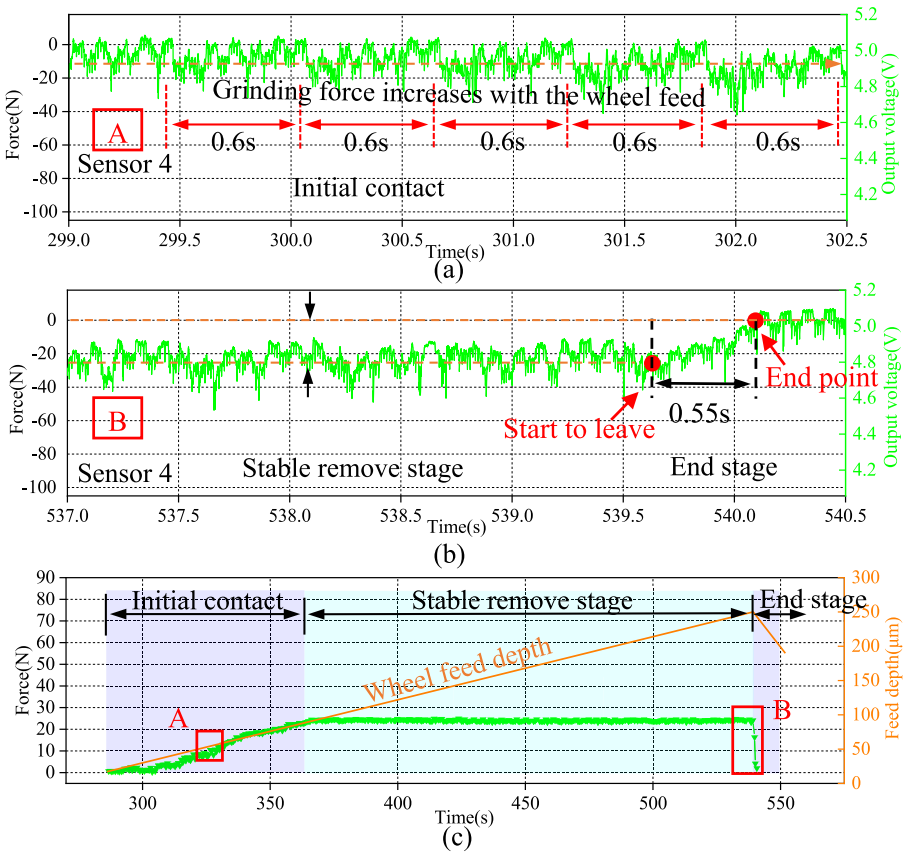

Fig. 9. Force variation of sensor 4 under condition (b). (a) initial contact stage; (b) stable remove stage & end stage; (c) variation of the grinding force at different grinding stages.

Table 3
Grinding force results (wafer speed N_w = 100 rpm).

Conditions	Feed rate f (μm/min)	Wheel speed N_s (r/min)	Sensor 1 (N, r = 90 mm)	Sensor 2 (N, r = 60 mm)	Sensor 3 (N, r = 30 mm)	Sensor 4 (N, r = 0 mm)
(a)	90	3000	90.60	73.40	61.21	30.03
(b)	60	3000	77.65	67.90	48.88	24.05
(c)	30	3000	70.03	50.32	43.21	17.51
(d)	60	2500	82.70	67.80	53.22	23.23
(e)	60	2000	86.47	73.06	58.53	27.01

Eq. (1) describes the relationship between the local removal amount of a single wheel segment and process parameters, geometric parameter as well as the radial distance of wafer. As described in Eq. (1), the local removal amount increases with feed rate of the grinding wheel and wafer radial distance and decreases with the spindle rotational speed. Fig. 12 shows the relationship between the grinding force (F_n) and the local material removal amount (V), which is calculated by Eq. (1). Since the force measured by the sensor 4 is the force at the stage when the wheel segment leaves and the grinding process is complex, which is not considered in the calculation. The value of the coefficient of determination R^2 is 0.92. It indicates a significant linear correlation exists between the grinding force and the local material removal amount.

3.4. Process parameters optimization based on the grinding force

Specific grinding energy, considered as a key indicator of grinding damage, is used to reflect the damage depth. Since the specific grinding energy is calculated through grinding force and process parameters, among which the grinding force is also related to the process parameters, the relationship between the grinding force and grinding damage depth can be obtain. By further considering the material removal efficiency, the process parameter optimization is proposed.

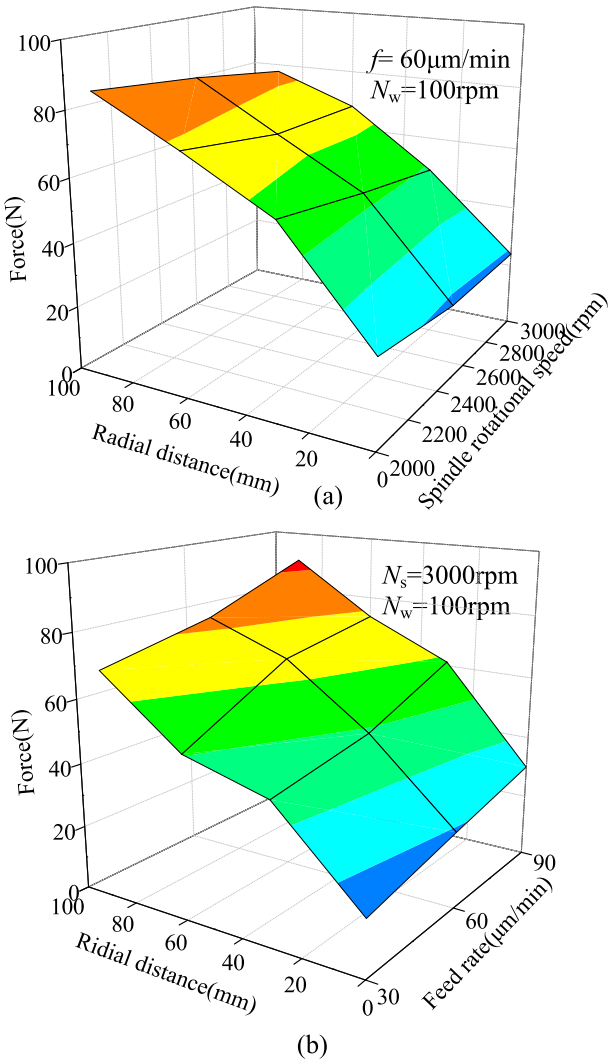

Fig. 10. Effects of process parameters on grinding force (a) spindle rotational speed; (b) wheel feed rate.

Bifano et al. [28] investigated the specific grinding energy of different brittle materials and indicated that the specific grinding energy can be used to in-process control of the grinding process as it can reflect the grinding damage depth. The specific grinding energy decreased with the increase of subsurface damage depth. The similar phenomenon was also found in Ref. [29]. For wafer self-rotating grinding, the specific grinding energy can be expressed as,

$$\mu = \frac{P}{Q(r)} = \frac{kF_n \cdot v_s}{Q(r)} = \frac{kF_n \cdot 2\pi R_s N_s}{Q(r)} \tag{2}$$

where P is the grinding power, F_n is the measured normal force acting on the segment, v_s is the linear speed of the wheel segment. k is the force ratio of tangential force F_t to normal force F_n, which depends on several parameters, e.g. grain material, grain size, random distribution of cutting grains and process parameters. Herein, an average cutting depth of grains model [5] and relationship between force ratio and cutting depth [30] were used to establish the variable force ratio. In Ref [5], the cutting depth model was developed, which considered the effects of grain size, random distribution of cutting grains, grain shape, and process parameters. The cutting depth can be calculated as,

$$d_c = 2.44\left(\frac{E_1}{E_0}\right)^n \left(\frac{1}{\mu}\right) R_e \left(\frac{r \cdot f \cdot N_w}{L \cdot W \cdot \gamma \cdot N_s^2 \left(1 + \frac{r^2}{8R_s^2}\right)}\right)^{0.4} \tag{3}$$

where d_c is the average cutting depth of the grains. E_1 and E_0 are the elastic modulus of the wheel bonding material and workpiece, respectively. μ is the ratio of removal depth to cutting depth. r is radial distance of wafer, f, N_s are wheel feed

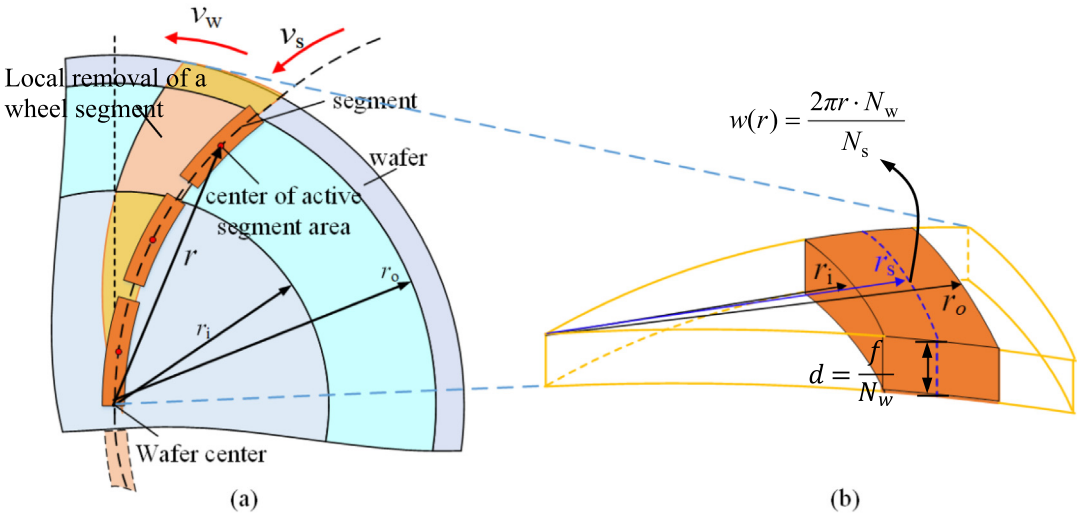

Fig. 11. Local removal amount during one revolution of grinding wheel. (a) Schematic diagram of the local removal; (b) enlarged view of local removal.

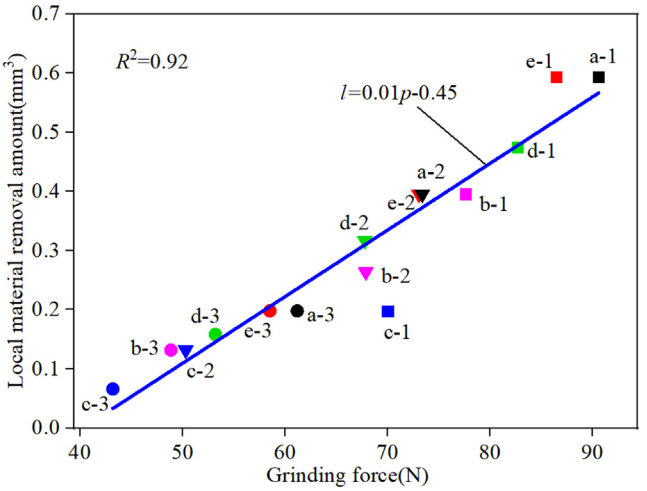

Fig. 12. Relationship between the grinding force and the local material removal amount. (For each data point, the letter represents grinding condition, and number represents sensor location).

rate and wheel rotational speed. L, R_s are the mean circumference and radius of grinding wheel, W is the width of the wheel segment, γ is the grain volume ratio. R_e is the average radius of grains.

In Ref. [30], the force ratio during scratching process of monocrystalline silicon wafer was investigated by tribometer. In which a diamond tip with 20 μm tip radius was used, this is consistent with the average grain size used in this paper. The empirical formula between the force ratio k and cutting depth d_c can be obtained by fitting the experimental value in Ref. [30] as,

$$k = 0.037 d_c^{0.40} \tag{4}$$

Combine Eq. (3) and Eq. (4), the force ratio under different process parameters can be obtained, as shown in Table. 4. $Q(r)$ is the local material removal rate (MRR), which can be obtained by the ratio of local removal amount to time,

$$Q(r) = 2\pi r f \cdot (l_s + l_g) \tag{5}$$

Substituting Eq. (5) into Eq. (2) gives,

$$\mu = \frac{k F_n \cdot R_s N_s}{r f \cdot (l_s + l_g)} \tag{6}$$

Table 4
Force ratio under different process parameters (wafer speed N_w = 100 rpm).

Conditions	Feed rate f (μm/min)	Wheel speed N_s (r/min)	Sensor 1 (r = 90 mm)	Sensor 2 (r = 60 mm)	Sensor 3 (r = 30 mm)
(a)	90	3000	0.25	0.23	0.21
(b)	60	3000	0.23	0.22	0.20
(c)	30	3000	0.21	0.20	0.18
(d)	60	2500	0.25	0.23	0.21
(e)	60	2000	0.27	0.25	0.22

Wheel parameters: L = 983 mm; W = 3.5 mm; R_e = 24 μm (#320); γ = 0.375; R_s = 156 mm; μ = 0.35; E_1 = 40GPa; E_0 = 130GPa [5].

Eq. (6) describes the effects of grinding force, process parameters and geometry parameters of the grinding wheel on specific grinding energy, where the grinding force is also a variable which is related to process parameters. Substituting the measured force (listed in Table 2), process parameter, and geometry parameters into Eq. (6), the specific grinding energy can be obtained, as shown in Fig. 13. The force measured by the sensor 4 is not considered.

Taking condition (c) as an example (Fig. 13), when the radial distance of the wafer increases from 30 mm to 90 mm, the specific grinding energy decreases from 113.84 J/mm^3 to 72.89 J/mm^3. It indicated that the specific grinding energy decreased with the increase of radial distance of wafer. By contrast, it can also be found from the Fig. 13 that the specific grinding energy decreased with the increase of spindle feed rate (condition (a)–(c)). With the increases of spindle rotational speed (condition (b), (d)–(e)), the specific grinding energy increased. The similar phenomenon was found in the grinding process of other brittle materials, e.g. BK-7 glass [31] and SiC ceramic [32]. Therefore, larger radial distances of wafer, higher wheel feed rates, and lower spindle rotational speeds mean that wafers produce greater subsurface damage (SSD) depth, which is consistent with our previous experimental observations [5].

The material removal efficiency is described in Eq. (5), which increased with the increase of spindle feed speed, but is independent of spindle speed. Therefore, on the premise of ensuring the machining efficiency, increasing the spindle speed can effectively reduce the damage. However, variation of specific grinding energy indicated that the machining damage depth increased with the increase of feed rate and decreases with the increase of spindle speed. For the actual grinding process, multi-step feed grinding can be used. In the initial grinding step, a larger feed rate can be used to improve machining efficiency, and at the end step of grinding, the spindle feed rate is reduced to ensure machining quality.

4. Conclusion

(1) A novel grinding force measurement device and method for silicon wafer self-rotating grinding process is developed. The method is achieved by embedding four thin film force sensors on a self-designed force measurement device and in situ monitoring through wireless signal transmission. Based on the proposed method, the grinding force of various process parameters are measured. The results indicate that the method has the advantages of high precision, low cost and convenient implementation.

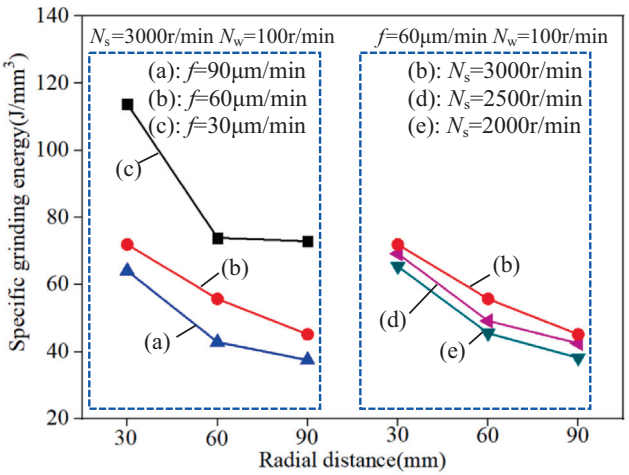

Fig. 13. Effect of grinding parameter on specific grinding energy.

(2) The change of grinding force in the whole grinding process is revealed for the first time. The grinding force distribution along radial distance of wafer and the effects of process parameters on grinding force are also investigated. The results show that the grinding force increases with the increase of spindle feed speed and wafer radial distance, decreases with the increase of spindle speed.
(3) Based on the measured grinding force, specific grinding energy, as an indicator of grinding damage, are calculated and analyzed. Considering grinding damage and machining efficiency, the optimization scheme of process parameters is proposed, which provides theoretical support for grinding process.

CRediT authorship contribution statement

Fei Qin: Conceptualization, Methodology, Project administration. **Lixiang Zhang:** Validation, Data curation, Writing - original draft. **Pei Chen:** Visualization, Investigation, Writing - review & editing. **Tong An:** Resources. **Yanwei Dai:** Software. **Yanpeng Gong:** Formal analysis. **Zhongbo Yi:** Investigation. **Haiming Wang:** Supervision.

Declaration of Competing Interest

The authors declare that they have no known competing financial interests or personal relationships that could have appeared to influence the work reported in this paper.

Acknowledgement

The author would like to deeply appreciate the financial support from the National Nature Science Foundation of China (Grant no. 11672009), and National Science and Technology Major Project (Grant no.2014ZX02504-001).

References

[1] P. Van Zant, Microchip Fabrication: A Practical Guide to Semiconductor Processing, fifth ed., McGraw-Hill, New York, 2004.
[2] Z.J. Pei, S.R. Billingsley, S. Miura, Grinding induced subsurface cracks in silicon wafers, Int. J. Mach. Tools Manuf. 39 (7) (1999) 1103–1116.
[3] Y. Mizushima, Y. Kim, T. Nakamura, R. Sugie, H. Hashimoto, A. Uedono, T. Ohba, Impact of back-grinding-induced damage on Si wafer thinning for three-dimensional integration, Jpn. J. Appl. Phys. 53 (5S2) (2014) 5.
[4] J. Sun, P. Chen, F. Qin, T. An, H. Yu, B. He, Modelling and experimental study of roughness in silicon wafer self-rotating grinding, Precis. Eng. 51 (2018) 625–637.
[5] L. Zhang, P. Chen, T. An, Y. Dai, F. Qin, Analytical prediction for depth of subsurface damage in silicon wafer due to self-rotating grinding process, Curr. Appl. Phys. 19 (5) (2019) 570–581.
[6] K.M.K.K. Kondo, Three-Dimensional Integration of Semiconductors: Processing, Materials, and Applications, Springer, 2015.
[7] Y.S. Kim, N. Maeda, H. Kitada, K. Fujimoto, S. Kodama, A. Kawai, K. Arai, K. Suzuki, T. Nakamura, T. Ohba, Advanced wafer thinning technology and feasibility test for 3D integration, Microelectron. Eng. 107 (2013) 65–71.
[8] Y.P. Tsai, Method of backside grinding a bumped wafer: U.S. Patent 7,235,426, 2007.
[9] R. Teti, K. Jemielniak, G.O. Donnell, D. Dornfeld, Advanced monitoring of machining operations, CIRP Ann.-Manuf. Techn. 59 (2) (2010) 717–739.
[10] J. Tang, J. Du, Y. Chen, Modeling and experimental study of grinding forces in surface grinding, J. Mater. Process Tech. 209 (6) (2009) 2847–2854.
[11] H. Chang, J.J.J. Wang, A stochastic grinding force model considering random grit distribution, Int. J. Mach. Tools Manuf. 48 (12–13) (2008) 1335–1344.
[12] U.S. Patnaik Durgumahanti, V. Singh, P. Venkateswara Rao, A new model for grinding force prediction and analysis, Int. J. Mach. Tools Manuf. 50 (3) (2010) 231–240.
[13] Z. Li, F. Zhang, X. Luo, X. Guo, Y. Cai, W. Chang, J. Sun, A new grinding force model for micro grinding RB-SiC ceramic with grinding wheel topography as an input, Micromachines-Basel 9 (8) (2018) 368.
[14] Y. Jeong, D. Cho, Estimating cutting force from rotating and stationary feed motor currents on a milling machine, Int. J. Mach. Tools Manuf. 42 (14) (2002) 1559–1566.
[15] Z.J. Pei, A. Strasbaugh, Fine grinding of silicon wafers: designed experiments, Int. J. Mach. Tools Manuf. 42 (3) (2002) 395–404.
[16] C.H. Lauro, L.C. Brandão, D. Baldo, R.A. Reis, J.P. Davim, Monitoring and processing signal applied in machining processes-A review, Measurement. 58 (2014) 73–86.
[17] Z. Xie, Y. Lu, J. Li, Development and testing of an integrated smart tool holder for four-component cutting force measurement, Mech. Syst. Signal Pr. 93 (2017) 225–240.
[18] E. Brinksmeier, C. Heinzel, L. Meyer, Development and application of a wheel based process monitoring system in grinding, CIRP Ann.-Manuf. Techn. 54 (1) (2005) 301–304.
[19] M. Sarma, F. Borchers, G. Dumstorff, C. Heinzel, W. Lang, Measuring strain during a cylindrical grinding process using embedded sensors in a workpiece, J. Sens. Sens. Syst. 6 (2) (2017) 331–340.
[20] Y. Zhao, Y. Zhao, C. Wang, S. Liang, R. Cheng, Y. Qin, P. Wang, Y. Li, X. Li, T. Hu, Design and development of a cutting force sensor based on semi-conductive strain gauge, Sensors Actuat. A Phys. 237 (2016) 119–127.
[21] L. Ma, S.N. Melkote, J.B. Morehouse, J.B. Castle, J.W. Fonda, Thin-film PVDF sensor-based monitoring of cutting forces in peripheral end milling, J. Dyn. Syst. Meas. Control. 134 (5) (2012) 51014.
[22] L. Ma, S.N. Melkote, On-ling monitoring of end milling forces using a thin film based wireless sensor module, Proceedings of the ASME 2010 International Manufacturing Science and Engineering Conference, USA, 2010.
[23] M. Luo, H. Luo, D. Axinte, D. Liu, J. Mei, Z. Liao, A wireless instrumented milling cutter system with embedded PVDF sensors, Mech. Syst. Signal Pr. 110 (2018) 556–568.
[24] D. Liu, Y. Hu, D. Zhang, H. Luo, Milling force monitoring with thin-film sensors integrated into fixtures, Int. J. Adv. Manuf. Technol. 103 (1–4) (2019) 1519–1527.
[25] J.A. Couey, E.R. Marsh, In-process force monitoring for precision grinding semiconductor silicon wafers, Int. J. Manuf. Technol. Manag. 6 (5/6) (2005) 430–440.
[26] D. Pähler, Measurement of local contact zone forces in rotational grinding of silicon wafers, I. J. Mecha. Manuf. Syst. 4 (6) (2011) 511–539.
[27] FlexiForce A201 Sensor <https://www.tekscan.com/products-solutions/force-sensors/a201>.
[28] T.G. Bifano, S.C. Fawcett, Specific grinding energy as an in-process control variable for ductile-regime grinding, Precis. Eng. 13 (4) (1991) 256–262.

[29] H. Masoumi, S.M. Safavi, M. Salehi, Grinding force, specific energy and material removal mechanism in grinding of HVOF-sprayed WC–Co–Cr coating, Mater. Manuf. 29 (3) (2014) 321–330.
[30] B. Bhushan, X. Li, Micromechanical and tribological characterization of doped single-crystal silicon and polysilicon films for microelectromechanical systems devices, J. Mater. Res. 12 (1997) 54–63.
[31] J. Dai, H. Su, T. Yu, H. Hu, W. Zhou, W. Ding, Experimental investigation on materials removal mechanism during grinding silicon carbide ceramics with single diamond grain, Precis. Eng. 51 (2018) 271–279.
[32] H. Kaliszer, Grinding technology. Theory and applications of machining with abrasives: S. Malkin, Ellis Horwood Ltd., Int. J. Mach. Tools Manuf. 31 (3) (1991) 435–436.